RESEARCH ARTICLE

Silica-based core materials for thermal superinsulations in various applications

Sebastian Sonnick[1] | Hermann Nirschl[2] | Matthias Rädle[1]

[1]Center for Mass Spectrometry and Optical Spectroscopy, Mannheim University of Applied Sciences, Mannheim, Germany

[2]Institute of Mechanical Process Engineering and Mechanics, Karlsruhe Institute of Technology, Karlsruhe, Germany

Correspondence
Sebastian Sonnick, Center for Mass Spectrometry and Optical Spectroscopy, Mannheim University of Applied Sciences, Paul-Wittsack-Straße 10, Mannheim 68163, Germany.
Email: s.sonnick@hs-mannheim.de

Summary

Vacuum insulation panels (VIP) are usually manufactured using standardized manufacturing processes based on empirical values and in most cases with any fumed silica as the main component of the core material. However, not all applications have the same requirements in terms of thermal conductivity and service life. Therefore, it is useful to adapt the kind of core materials and their product specifications, such as particle size and porosity, to the different applications. Furthermore, in some applications cheaper core materials, like precipitated silica, would be a reasonable alternative. To replace the time-consuming series of measurements for this purpose, this work offers comprehensive parameter studies to determine the optimum product properties of precipitated silica, fumed silica, silica gel, and glass spheres for use in the building sector, in transport boxes, as a superinsulation at atmospheric pressure, and as a switchable VIP. As a result, not only the preferred materials but also their porosities and particle sizes are presented. For atmospheric pressure and construction applications, fumed silica has to be preferred. For the transport sector and switchable VIPs as well as certain special applications, precipitated silica and silica gel may well be reasonable alternatives.

KEYWORDS

effective thermal conductivity, silica-based core materials, superinsulations, vacuum insulation panel

1 | INTRODUCTION

In times of climate change, efficient thermal insulation that is precisely tailored to the various applications is essential. The aim is not only to reduce the heat flux as much as possible but also to save space. With the goal to generate more usable volume in homes, transport boxes, heat storage units, or any other conceivable application, so-called superinsulations are becoming increasingly popular.[1] They are characterized by the fact that their thermal conductivities are lower than that of resting air,[2] that is, less than $0.026 \frac{W}{mK}$. The most common superinsulations are vacuum insulation panels (VIP) and aerogels. The most widely used core material for VIPs is fumed silica.[3] However, since this material is very expensive and thus increases the overall price of the insulation, scientists are searching for viable alternatives.[4] For this purpose, inexpensive filler materials[5] or even waste materials[6] are added to the fumed silica to lower the price. However, alternative materials such as foams[7] or

fibers[8] are also being investigated and used in some cases.[9] Silica aerogel is the most promising material for atmospheric pressure superinsulation and is therefore intensively studied.[10] However, it is very high price makes it uneconomical for many applications. Therefore, this work also investigates alternative silica-based materials that may represent a cost advantage over traditionally used materials for both vacuum and atmospheric pressure applications. Glass fiber-based VIP cores are also a low-cost silica-based alternative.

They are primarily used for short-term applications. However, since the calculation models used in this work refer to particulate systems only, glass-fiber-based VIPs are not discussed. In addition to the physical and technical requirements, there is growing interest in sustainable[11] or oil-free alternative materials.[12] Insulation materials based on amorphous silica, such as fumed or precipitated silica, silica gel (silica xerogel), or sometimes even glass spheres can optimally meet these requirements. On the other hand, it is known from Resalati et al[13] that especially fumed silica has a very high environmental impact due to its energy-intensive production. Therefore, this work examines also alternative silica-based materials in more detail and, for the first time, recommendations are given for their product properties to be targeted for the various applications of superinsulations.

By definition, a superinsulator can only exist due to the so-called Knudsen effect. It states that the thermal conductivity of a gas, for example, in the pore of an insulating material, decreases significantly when the mean free path of the gas molecules becomes larger than the surrounding space, that is, the pore. The ratio of the mean free path length L to the size of the void space x is therefore called Knudsen number Kn. To achieve a significant reduction in thermal conductivity, either the gas pressure can be reduced or the pore size can be decreased. This effect is used, for example, in vacuum insulation panels. Here, porous, open-pore core material is formed into a panel shape and sealed under a vacuum using a barrier film. In some materials, such as some kinds of silica, the Knudsen effect is already achieved at atmospheric pressure, since at least some of the pores are of the same size as the mean free path of air molecules (approx. 68 nm). Although this fundamental relationship is clear since Knudsen,[14] the applicability of the corresponding analytical calculation models for real porous media is not yet fully understood.[15] Heat transfer in porous media is mainly composed of three mechanisms: gas thermal conductivity λ_g, solid thermal conductivity λ_s, and radiation λ_r. Moreover, a coupling λ_c between the above mechanisms must be considered which strongly depends on the microstructure of the materials. In

particular, the ratio between gas thermal conductivity and the resulting coupling with the solid phase is difficult to capture for chaotic structures. It depends on the Knudsen number and can make the largest overall contribution to the total heat transfer. There are many different calculation models, especially for the gas and coupling contribution in the literature some of which give very different results.

Therefore, in their last publication,[16] the authors presented a selection guide for such models specifically for the material groups fumed silica (FS), precipitated silica (PS), silica gel (SG), and glass spheres (GS). From a total of 2800 possible combinations of analytical models for the calculation of the effective thermal conductivity and the gas thermal conductivity, the one with the best agreement with the measurement results was determined. Thus, it is possible to predict the gas pressure-dependent thermal conductivity for the mentioned substances with an average deviation of about 10% without any parameter adjustment or fitting. As input parameters, the thermal conductivities of the two phases (solid λ_p and gas λ_g), the porosity ϕ, the mean particle size D, and the pore size distribution d_{dist} are required. To be able to predict the thermal conductivity of potential insulation materials as reliably as possible using analytical methods, the correct models must be used. Combining these gas thermal conductivity models with common ones for solid conductivity and radiation, it is possible to determine the optimal product specifications of fictitious silica-based core materials for different requirements.

Contrary to a large number of calculation models for the different heat transfer mechanisms in general, there are not many attempts in the literature to predict the gas pressure-dependent thermal conductivity in a product-specific way. Verma et al[17] used numerical methods to predict the effective thermal conductivity of perlite with different product specifications. They were able to classify the result between the two ideal cases "hexagonal packing" and "simple cubic packing." Rottmann et al[18] also developed a model for perlite. They used several fitting parameters to get a good agreement with measurements between 293 and 1073 K. Bi et al[19] present a model specifically for aerogels which, taking into account porosity and particle size, provides good agreement with measured values. Generally, the research activity in the field of aerogels is very strong. Singh et al[20] describe the heat transfer mechanisms in different fumed silica. However, neither the density nor the particle size is taken into account when calculating the gas contribution. In this respect, the present paper shows clear advantages. Thus, for the first time, the various calculation models and input parameters can be optimally assigned to the materials mentioned to precisely investigate the influences of

the different product specifications. For this purpose, parameter studies are presented in which the gas pressure-dependent thermal conductivity is calculated for the mentioned materials as a function of particle size and porosity. The results are evaluated according to different criteria for the applications: VIPs for the building sector, VIPs for transport boxes, atmospheric pressure superinsulations, and switchable VIPs. Finally, recommendations are made for optimal product properties for the production of tailor-made VIPs or superinsulations.

2 | CALCULATION METHODS

First, the calculation methods for determining the individual heat transfer components and finally the models used for the effective thermal conductivity will be presented. The calculation procedure differs for all materials. This will be explained in more detail below. All calculations, as well as the measurements, are performed at a constant mean temperature of 30°C. Furthermore, dry gases with zero humidity are used.

2.1 | Gas thermal conductivity

For the calculation of the thermal conductivity of a Knudsen gas the common equation according to Prasolov is used.[21] It is shown in Equation (1) where λ_0 is the thermal conductivity of the gas at atmospheric conditions, β is a dimensionless factor, and Kn is the Knudsen number.

$$\lambda_g = \frac{\lambda_0}{1 + \beta Kn} \qquad (1)$$

The Knudsen number is the ratio between the mean free path of gas molecules L and a characteristic geometric quantity $x \left(Kn = \frac{L}{x} \right)$. The mean free path can be calculated using Equation (2).

$$L = \frac{k\ T}{\sqrt{2}\ \pi\ d_{kin}^2\ p} \qquad (2)$$

The selection of the geometric size x, on the other hand, raises some questions. Therefore, in the previous study[16] it was investigated which measured values should be used for the individual material classes to obtain the most realistic results. The pore size, pore size distribution, and different particle sizes are available for selection, each with and without various corrections. Another controversial topic is the calculation of the dimensionless factor β. Most promising calculation methods for
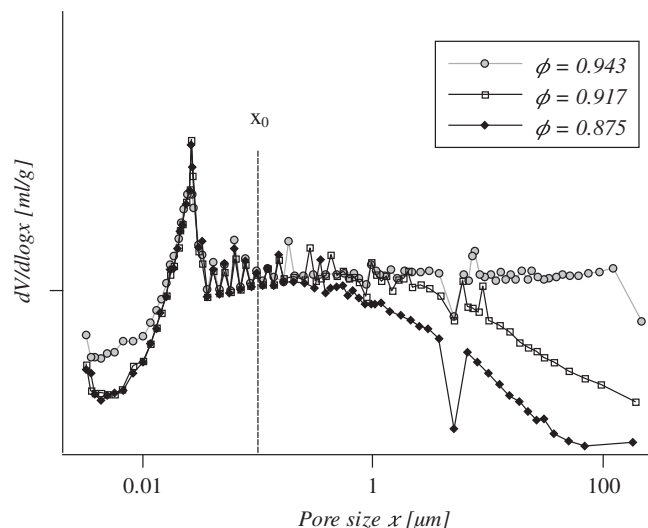

FIGURE 1 Pore size distributions measured with mercury intrusion porosimetry of the same precipitated silica sample which was treated with different amounts of pressure beforehand

different material classes could be determined as favorites in the preliminary study and can now be used accordingly.

2.1.1 | Pore size distribution

For many materials it has proven to make sense to consider the pore size distribution for the geometric parameter x in Equation (1). For this purpose, an individual thermal conductivity is calculated for each pore size that occurs and summed up over its volume fraction. In parameter studies, however, this is difficult to implement, since the pore size distribution is inseparably related to the porosity and the particle size. Nevertheless, to be able to work with distributions, a method is used to determine the pore size distribution of a certain sample with a certain particle size as a function of the porosity. For this purpose, only one measurement curve recorded with mercury intrusion porosimetry (MIP) at any porosity is required. Mechanical compaction of the powders does not affect all pore sizes equally. Logically, the largest pores disappear first. Investigations on samples compressed to different porosities have shown that the pores below a certain limit are not affected at all or only very slightly by the mechanical compaction. For clarification, the pore size distributions of the same precipitated silica which was compressed to different degrees are shown in Figure 1.

The threshold value up to which the pores are influenced by mechanical compression is related to the smallest particle unit connected by real material bridges. Therefore, the aggregate size is a good guide value for the
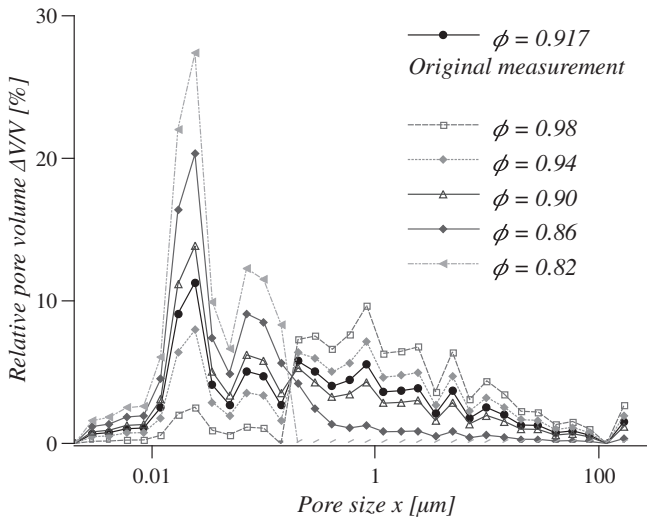
FIGURE 2 Relative pore size distributions of precipitated silica calculated with Equations (3) and (4)

materials investigated here. To calculate the pore size distribution as a function of porosity, the measured relative pore size distribution $\frac{\Delta V}{V}(\phi_1)$ at arbitrary porosity ϕ_1 is used as a basis. Then, a pore size x_0 is chosen below which no influence of compression on the pores is assumed. Initially, the aggregate size can be used here. To determine the relative pore size distribution $\frac{\delta V}{V}(\phi_2)$ Equation 3 is applied for all pore size fractions $\overline{x} < x_0$ while for all $\overline{x} > x_0$ Equation 4 can be used.

$$\frac{\Delta V}{V}(\overline{x} < x_0, \phi_2) = \frac{\Delta V}{V}(\phi_1) \times \frac{\phi_1}{\varphi^*} \quad (3)$$

$$\frac{\Delta V}{V}(\overline{x} > x_0, \phi_2) = \frac{\Delta V}{V}(\phi_1) \times \phi_1 - F\phi^* \left(\frac{\Delta V}{V}(\phi_1) \times \phi_1 \right.$$
$$\left. - C_1 b^{10^6(x - x_0)} \right) \quad (4)$$

Here, $\frac{\Delta V}{V}$ is the relative volume fraction of a given pore size fraction $\overline{x}$, ϕ_1 is the original porosity of the measured sample, ϕ_2 is the porosity to be calculated, C_1 is the relative volume fraction of the pore size fraction x_0, and $b = 10^{-4}$. Factor F is fitted with the condition $\sum \frac{\Delta V}{V}(\phi_2) = \sum \frac{\Delta V}{V}(\phi_1)$. The ratio ϕ^* can be called apparent porosity and is calculated via Equation (5).

$$\phi^* = \frac{\phi_2(1 - \phi_1)}{(1 - \phi_2)} \quad (5)$$

This method works only for $\sum \frac{\Delta V}{V}(\overline{x} < x_0, \phi_2) < \sum \frac{\Delta V}{V}(\phi_1)$. If this condition is only slightly missed, a smaller x_0 can

possibly be chosen. In the present work, the following values for x_0 were found to be useful: fumed silica ($x_0 = 70$ nm), precipitated silica ($x_0 = 100$ nm), and silica gel ($x_0 = 200$ nm). The pore size distributions of precipitated silica with porosities between 0.8 and 0.98 result from Equations (3) and (4) are shown as an example in Figure 2. For glass beads, the measurement of the pore size distribution by MIP proved to be inappropriate. Therefore, the calculation of the characteristic geometric size x from the particle size using Kozeny's correction[22] is used instead.

2.1.2 | Dimensionless coefficient β

The dimensionless parameter β depends primarily on the thermal accommodation coefficient α and thus on the temperature jump at the gas/solid boundaries in the porous material. It can be described with different analytical equations from the literature, which can sometimes lead to considerably different results. It has been shown that the equations are preferred depending on the material under investigation. The exact relationships are described in Sonnick et al.[16] In Table 1, the most promising equations for α and β for the individual materials are listed accordingly.

2.2 | Radiation

The radiative transfer portion of the total heat conduction can be calculated as a diffusion process if the optical thickness of the porous material is large over the entire wavelength range of interest and the mean free path of photons is small compared to the distance over which significant temperature changes occur.[28] This can be assumed for all technical relevant silica-based insulation materials. Thus, it is possible to specify a radiation-induced fraction of the total heat transfer in terms of a radiative thermal conductivity λ_r. It can be calculated by use of the Rosseland diffusion approximation[29] according to Equation 6.

$$\lambda_r = \frac{16\sigma n^2}{3\hat{E}(T, \phi)} T_{rad}^3 \quad (6)$$

Here, σ is the Stefan-Boltzmann constant, n is the refractive index (which can be assumed to be one of the materials considered in this work[2]). $\hat{E}$ is the Rosseland average of the extinction coefficient. It is an average over all $E(\Lambda)$ which is weighted by the blackbody spectrum of the temperature of interest. It can be calculated according to Siegel and Hawell[30] via Equation (7).

TABLE 1 Recommended methods to calculate α and β for different porous media according to Sonnick et al[16]

Material	α	β
Precipitated silica	$\alpha = 1 - \frac{144.6}{(M_G+12)^2}$	$\beta = 2 \times \frac{2-\alpha}{\alpha} \frac{2\kappa}{\kappa+1} \frac{1}{Pr}$
Fumed silica	$\alpha = 1 - \left(\frac{M_S-M_G}{M_S+M_G}\right)^2$	$\beta = 2 \times \frac{2-\alpha}{\alpha} \frac{2\kappa}{\kappa+1} \frac{1}{Pr}$
Silica gel	$\alpha = 1 - \frac{144.6}{(M_G+12)^2}$	$\beta = \frac{2-\alpha}{\alpha} \frac{2\kappa}{\kappa+1} \frac{1}{Pr}$
Glass spheres	$\alpha = exp\left[C_0\left(\frac{T-T_0}{T_0}\right)\right]\left(\frac{M_G^*}{C_1+M_G^*}\right) + \left\{1 - exp\left[C_0\left(\frac{T-T_0}{T_0}\right)\right]\right\} \frac{2.4\frac{M_G}{M_S}}{\left(1+\frac{M_G}{M_S}\right)^2}$	$\beta = \frac{5\pi}{16} \frac{9\kappa-5}{\kappa+1} \frac{2-\alpha}{\alpha}$

Notes: Original references PS: α^{23}, β^{24}; FS: α^{24}, β^{24}; SG: α^{23}, β^{25}; GS: α^{26}, β.[27]

$$\frac{1}{\hat{E}(T)} = \sum_{\Delta\Lambda} \frac{\frac{1}{E(\Lambda)}f_\Lambda(T)\Delta\Lambda}{\sum_{\Delta\Lambda} f_\Lambda(T)\Delta\Lambda} \quad (7)$$

with

$$f_\Lambda(T) = \frac{\pi C_3 C_4}{2\Lambda^6} \times \frac{1}{\sigma T^5} \times \frac{\exp\left(\frac{C_4}{\Lambda T}\right)}{\left[\exp\left(\frac{C_4}{\Lambda T}\right) - 1\right]^2} \quad (8)$$

where $C_3 = 5.9544 \times 10^{-17} \frac{W}{m^2}$ and $C_4 = 1.4388 \times 10^{-2}$ mK.

The average radiation temperature T_{rad} is defined by the two wall temperatures T_1 and T_2 using Equation (9). In this work, 45 and 15°C were used for T_1 and T_2, respectively, as the thermal conductivity measurements were carried out with these temperatures.

$$T_{rad}^3 = \frac{T_1^4 - T_2^4}{4(T_1 - T_2)} \quad (9)$$

The spectral extinction coefficient $E(\Lambda)$ can be obtained by spectroscopic measurements determining the transmittance as a function of the sample length.[31] This procedure is shown in Section 3.2.

2.3 | Solid thermal conductivity

The heat transfer across the solid backbone of a particle bed is strongly influenced by the particle-particle contact areas. Assuming elastic deformation of the particles in the contact regions, the Hertz contact theory can be applied to calculate the solid thermal conductivity λ_s[24] using Equation (10).

$$\lambda_s = 3.44(1-\phi)^{\frac{4}{3}}\left(\frac{1-\eta^2}{Y}\right)^{\frac{1}{3}}\lambda_P F^{\frac{1}{3}} \quad (10)$$

Here, η is the Poisson's ratio, Y the elastic modulus, and F the pressure load caused by at least the weight of the powder itself and sometimes, like in the case of vacuum insulation panels, by an additional external pressure load.

2.4 | Effective thermal conductivity

The macroscopic proportionality factor describing the heat flow through a dispersed medium at a certain temperature difference is called effective thermal conductivity λ_{eff}. It is not a "true" material value but is composed of the thermal conductivities of the individual components as well as many other influencing parameters. For porous media, there are numerous mathematical models for λ_{eff}. In the following, they will also be referred to as ETC models. On the one hand, they describe the interaction between the individual conductivities, in this case λ_s and λ_g, which is also referred to as the coupling effect or coupling conductivity λ_c. On the other hand, the ETC models are used to weight the individual components according to the porosity ϕ. In the preliminary study[16] mentioned above, the most common ETC models from the literature were investigated and classified with regard to the materials investigated. The most promising model for each material is used for the present parameter studies as well.

2.4.1 | Precipitated silica, silica gel, and glass spheres

For the material groups PS, SG, and GS, a model is used which is based on a cylindrical unit cell of two touching hemispheres with the simplifying assumption of parallel heat flow lines. It was developed by Swimm et al[32] and is based on a parallel connection of finitely small cylindrical shells of the mentioned unit cell. Each cylindrical shell is calculated as a series connection of the solid and

gas fractions applicable to the corresponding radius. In this process, a separate Knudsen number is calculated for each cylindrical shell according to the height of the gas fraction and thus an individual gas thermal conductivity is obtained.

$$x(i) = D - 2\sqrt{R^2 - \left(\frac{i}{N}R\right)^2} \qquad (11)$$

In 11 $D - x(i)$ is the void distance of the ith cylindrical shell, N is the total number of cylindrical shells, and D and R are diameter and radius. At this point, different measurement values should be used for D and R for the different materials. For PS, SG, and GS it has proven to be purposeful to use the largest conglomerates perceptible as individual particles accordingly. Glass beads are not multiscale. Therefore, the simple particle size or primary particle size is used here. Silica gel consists of aggregates which in turn are composed of small sintered primary particles. Here, the aggregate size has to be selected. Precipitated silica even has a three-stage structure. Here, the aggregates, driven by different adhesive forces, form the so-called agglomerates. Consequently, in the case of PS, the average agglomerate diameter for D in Equation (11) should be used.

$$\lambda_c = \frac{2}{R\pi} \sum_{i=1}^{N} A_i \left(\frac{D - x(i)}{\lambda_{g'}} + \frac{x(i)}{\lambda_p}\right)^{-1} \qquad (12)$$

The coupling thermal conductivity λ_c is the reciprocal sum of the individual shells, weighted by the respective area fraction A_i. $\lambda_g{}'$ is the gas thermal conductivity of the individual shells. To calculate the effective thermal conductivity of the porous material, the thermal conductivity of the pure gas phase λ_g and that of the unit cell λ_c are weighted according to a corrected porosity ϕ_{corr} as shown in Equation (13).

$$\lambda_{eff} = \lambda_{base} + \phi_{corr}\lambda_g + (1 - \phi_{corr})\lambda_c \qquad (13)$$

The corrected porosity ϕ_{corr} results from the porosity of the unit cell and the porosity of the investigated material ϕ.

$$\phi_{corr} = \frac{3\phi - 1}{2} \qquad (14)$$

2.4.2 | Fumed silica

For fumed silica, the ETC model of Zehner and Schlünder[33] gives the best results. Like the sphere model of

Swimm et al it is a unit cell model with consideration of local Knudsen numbers. The difference is that the surface of the model particles is not described by the sphere function, but by Equation (15).

$$r^2 + \frac{z^2}{(B - (B-1)x)^2} = 1 \qquad (15)$$

where

$$B = C\left(\frac{1 - \phi}{\phi}\right)^{\frac{10}{9}}$$

The local Knudsen number is given as a function of the radius with $Kn^* = \frac{Kn}{(1 - x(r))}$. Integration over r leads to Equation (16) which can be used to calculate the coupling conductivity.

$$\lambda_c = \lambda_0 \frac{2}{N-M} \left\{ \frac{\left[N - (1 + Kn)\frac{\lambda_0}{\lambda_p}\right]B}{(N-M)^2} \ln\frac{N}{M} \right.$$

$$\left. - \frac{B-1}{N-M}(1 + Kn) - \frac{B+1}{2B}\frac{\lambda_p}{\lambda_0}[1 - (N-M) - (B-1)Kn] \right\} \qquad (16)$$

with

$$M = B\left[\frac{\lambda_0}{\lambda_p} + Kn\right]$$

and

$$N = 1 + Kn$$

Zehner and Schlünder proposed different correction factors C for differently shaped particles. For example, $C = 1.25$ is recommended for spheres. Since no recommendation is available for irregularly shaped fumed silica particles, $C = 1.25$ is assumed here. The aggregate size is used to calculate the Knudsen number to adequately describe the size of the gap in which the coupling thermal conductivity occurs. The consideration of thermal radiation in the original model was neglected here since it is calculated separately. Using the corrected porosity $(1 - \sqrt{1 - \phi})$ the effective thermal conductivity can be calculated with Equation (17).

$$\lambda_{eff} = \left(1 - \sqrt{1 - \phi}\right)\lambda_g + \sqrt{1 - \phi}\lambda_c \qquad (17)$$

3 | MEASUREMENTS

Although this work is mainly theoretical, some measurements are required for the determination of input parameters and validations. Fourier transform infrared (FTIR) spectroscopy was performed to determine the emission coefficient of the materials and ultimately to determine λ_r. Furthermore, measurements of thermal conductivity at very low pressures are performed to validate the results of the calculations of λ_s and λ_r. The gas thermal conductivity and the coupling effect have already been extensively validated in the mentioned preliminary study. For the measurements, 15 different powdery samples including fumed and precipitated silica, silica gel, and glass spheres were used. The specifications of the materials including primary particle size, aggregate size, agglomerate size, porosity, and pore size distribution have been measured with small angle X-ray scattering, dynamic light scattering, laser diffraction, and MIP, respectively and can be taken from.[16]

3.1 | Solid and radiation thermal conductivity

At very low pressures or large Knudsen numbers ($Kn \gg 1$), the gas thermal conductivity can be completely neglected. Thus, there is no coupling between the gas and solid phases and only the radiative thermal conductivity and the solid thermal conductivity remain. Consequently, the sum of these two components can be determined by thermal conductivity measurements at very low pressures. The following equation applies:

$$\lambda_{base} = \lambda(p_{min}) = \lambda_s + \lambda_r \tag{18}$$

The samples to be analyzed were measured in a vacuum guarded hot plate apparatus. For this purpose, the apparatus was vacuumed to the maximum possible level overnight (approx. 0.05 mbar) and the sample was dried completely so that no moisture was left. In this condition, the values for λ_{base} were recorded.

The cooling and heating plate temperatures were 15 and 45°C, respectively, resulting in a mean measurement temperature of 30°C. The central measuring area of the guarded hot plate is $(8 \text{ cm})^2$. The entire plate including the guard ring is $(16 \text{ cm})^2$. The samples are mechanically compacted directly in the measuring chamber using a hydraulic press to a sample thickness between 6 and 8 mm. A detailed description of the measurement apparatus and error analysis can be found in.[34]

3.2 | Extinction coefficient

The determination of the average extinction coefficient $\hat{E}$ is fundamental for the calculation of the radiation thermal conductivity λ_r. Thus, transmission spectroscopy measurements have been performed using an FTIR spectrometer (*Bruker ALPHA II*). The samples were pressed onto a thin polyethylene film using a self-developed pressing device. This resulted in small platelike bodies with a thickness in the order of 100 μm. The polyethylene film was used as a support material and thus also for the background measurement. The result of the measurements is a spectrum $E(\Lambda)$. Where Λ is the wavelength. The mass of the sample and the diameter of the pressing device can be used to determine the area density m_a. To obtain the mass-specific extinction coefficient E_m, the average extinction coefficient $\hat{E}$ from Equation (7), which can be calculated from the measured $E(\Lambda)$ spectra, must be divided by m_a. To get the radiation thermal conductivity λ_r as a function of the porosity one can extend Equations (6) to (19) as follows.

$$\lambda_r = \frac{16\sigma n^2}{3 E_m \rho_s (1-\phi)} T_{rad}^3 \tag{19}$$

where ρ_s is the density of the non-porous solid skeleton. In the case of silica-based materials $\rho_s = 2200 \frac{kg}{m^3}$.[35] The bulk density of the porous materials is given by $\rho = \rho_s(1-\phi)$.

4 | RESULTS AND DISCUSSION

We first discuss the results for λ_s and λ_r. Then, the parameter studies of the effective thermal conductivity of the different materials are evaluated. Finally, their relevance to the various applications of superinsulations is discussed.

4.1 | Solid and radiation thermal conductivity

The results for the radiation thermal conductivities obtained with Equation (19) using the spectroscopic measurement results are shown in Figure 3. The λ_r values are plotted against the porosity of the measured materials. Each circle represents a silica-based material. The density which was used for the calculations is the same as for the thermal conductivity measurements. Standard deviations are plotted as error bars which are only visible as lines in the data points. The dotted line in Figure 3 was fitted to
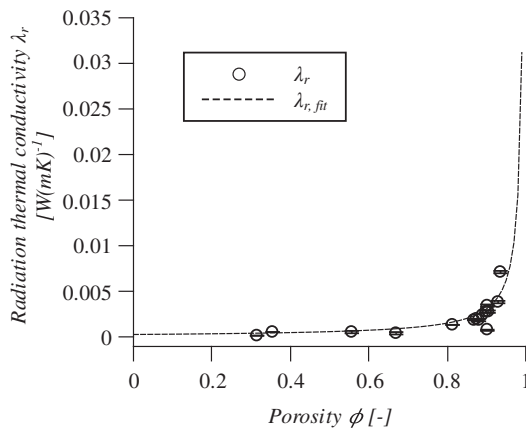
FIGURE 3 Calculated radiation thermal conductivity over porosity of silica-based materials. Circles: Calculated via Equation (19) using measured extinction coefficients; Dashed line: Calculation with fitted E_m
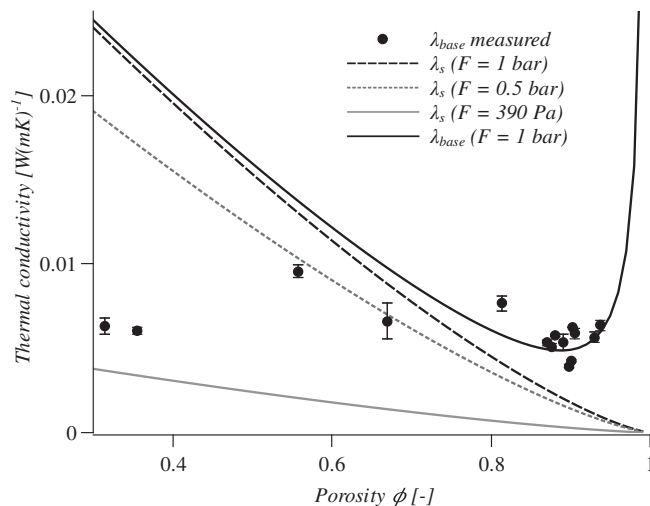

FIGURE 4 Calculated λ_s curves for different amounts of mechanical load F, calculated λ_{base} for $F = 1$ bar, and measured λ_{base} values for all samples investigated over porosity

the data points using the mass-specific extinction coefficient E_m as a fitting parameter. The procedure leads to Equation (20) for the porosity-dependent radiation thermal conductivity of silica-based powders at wall temperatures $T_1 = 45°C$ and $T_2 = 15°C$.

$$\lambda_r = \frac{3.118 * 10^{-4}}{(1 - \phi)} \qquad (20)$$

To calculate λ_{base}, the solid thermal conductivity λ_s has to be determined as well. It can be calculated as already mentioned via Equation (10). One decisive factor is the mechanical load F of the powder bulk. Three curves for the solid thermal conductivity calculated with

$F = 1$ bar, $F = 0.5$ bar, and $F = 390$ Pa are shown in Figure 4. A 390 Pa corresponds approximately to the load to which the samples were subjected during the thermal conductivity measurements. 1 bar, on the other hand, corresponds to the load on a VIP by atmospheric pressure. Furthermore, in Figure 4, the measured values for λ_{base} of all investigated materials are shown. Finally, a calculated curve for λ_{base} is shown, which is the sum of $\lambda_s(F = 1\ bar)$ and λ_r. It is found that the measured values of the materials with porosities greater than 0.8 agree relatively well with the calculated curve ($\lambda_{base}(F = 1$ bar)). However, the lower the porosity, the further the measured values move away from the calculated curve. The main reason for this is the assumed mechanical load because to achieve a smooth surface and the desired porosity, the samples were compacted before the thermal conductivity measurement. For this purpose, approx. 4 bar of compression pressure was applied. During this process, the pressed samples with higher porosities, such as from FS, PS, and some silica gels, deform plastically. The very small particles of these materials approach each other during the pressing process and are then held together for example by van der Waals forces, electrostatic interactions, or simple form closure. This attraction affects the solid thermal conductivity like a mechanical load from outside. Powders with higher porosities, such as glass beads, merely deform elastically during sample preparation. Their particles are too large to be significantly affected by the above-mentioned attractive forces and too spherical for form closure. During the measurement, only 390 Pa weight on the samples, which then have relatively low solid thermal conductivity if they have low porosity at the same time. Nevertheless, for the further calculations of all materials the curve $\lambda_{base}(F = 1$ bar) is used because in the scenario of a VIP, the atmospheric pressure weights equally on all materials.

4.2 | Effective thermal conductivity

In Sections 4.2.1 to 4.2.4, the results of the calculation of the effective thermal conductivity for the investigated materials are presented and discussed. Parameter studies were performed on the particle size relevant to the corresponding materials, as well as on the porosity. The chosen value domains are based on measurements, so that realistic ranges of the material data are studied in each case. The chosen domains can be found in Table 2. The different types of particle sizes (primary particles, aggregates, and agglomerates) are specified due to the different multiscalarities of the materials as well as the preferred calculation methods for each material according to.[16]

TABLE 2 Selected domains for the parameter study on porosity and the decisive particle size

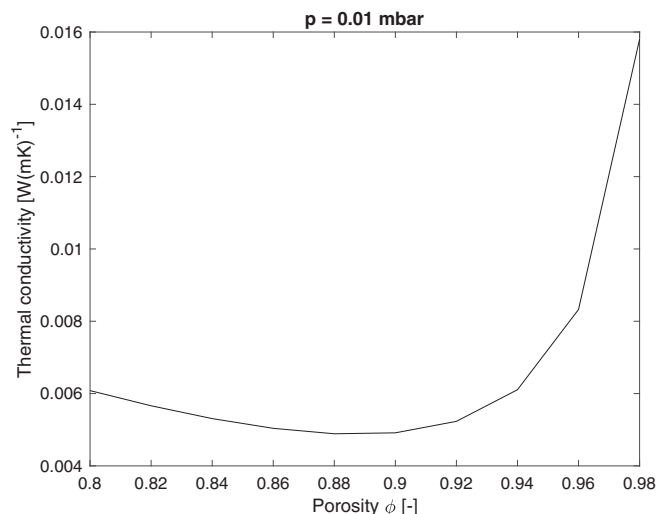|	PS	FS	SG	GS
Porosity	0.80 to 0.98	0.80 to 0.98	0.80 to 0.98	0.3 to 0.7
Particle size	Agglomerates	Aggregates	Aggregates	Primary particles
	5 to 40 μm	50 to 225 nm	5 to 40 μm	1 to 100 μm

FIGURE 5 Calculated thermal conductivity values over porosity for $P = .01$ mbar. Under the assumptions made, this curve applies in principle to all materials and particle sizes investigated

Porosity is used in the calculation both to determine the pore size distribution (Section 2.1.1) and as an input parameter for the corresponding ETC model (Section 2.4). For all materials, it is equally true that the lowest thermal conductivity can be achieved at the lowest possible pressure and a porosity of 0.89. This applies to all materials, since λ_{base} does not depend on particle or pore size but only on porosity, at least under the assumptions made. It was calculated with $P = 0.01$ mbar, and is shown in Figure 5 as a function of the porosity. The results are valid for all materials investigated.

In the following subsections, the results of the parameter studies for the pressure levels $P = 100$ and $P = 1000$ mbar of the individual materials are shown in Figures 6–9, respectively. In Section 4.2.5, the advantages and disadvantages of the individual materials for different applications are discussed.

4.2.1 | Precipitated silica

The thermal conductivity of precipitated silica at high gas pressures and small porosities is characterized by a strong coupling effect λ_c. As shown in Figure 6, the curves from the direction of small porosities come from a very high level, then drop down to the minimum value and rise

again due to increased gas thermal conductivity and a rapidly increasing radiation fraction in the direction of $\phi = 1$. The optimum porosity, that is, the one with the lowest thermal conductivity, increases with increasing pressure. For the smallest investigated particle size of 5 μm, the minimum values are obtained at $\phi = 0.86$ for $P = 100$ mbar and $\phi = 0.92$ for $P = 1000$ mbar. We can also observe that the optimum porosity also increases with increasing agglomerate size. This is due to the fact that the coupling effect is more pronounced for larger particles than for small ones, and the coupling contribution for precipitated silica depends approximately linearly on the porosity.[34]

4.2.2 | Fumed silica

For fumed silica, a significantly reduced tendency for coupling between λ_s and λ_g is observed compared to the other materials investigated. Therefore, it has proven useful to use aggregate size instead of agglomerate size as the unit cell size of the ETC model, since smaller particles provide less coupling than larger ones in the pressure range investigated. Here, again, the tendency that the optimum porosity also increases with increasing particle size can be observed. However, since the particles studied are much smaller than for PS, the optimum porosities are also much smaller. For FS, the porosity has a comparatively small effect on the effective thermal conductivity, especially in the range of common aggregate sizes of about 150 nm. Here, in the porosity area from $\phi = 0.82$ to $\phi = 0.9$, the decreasing coupling effect and the increasing radiative and gaseous thermal conductivity fractions seem to cancel each other out to a large extent.

4.2.3 | Silica gel

Although here the usual aggregate sizes are in the same order of magnitude as the agglomerates of the precipitated silicas, one does not achieve as low thermal conductivities for silica gels as for PS, especially in the higher pressure ranges. At the model level, this is obviously related to the calculation method for β. The factor of 2 in the formula used for PS leads to significantly lower gas thermal conductivities. In reality, this effect is probably
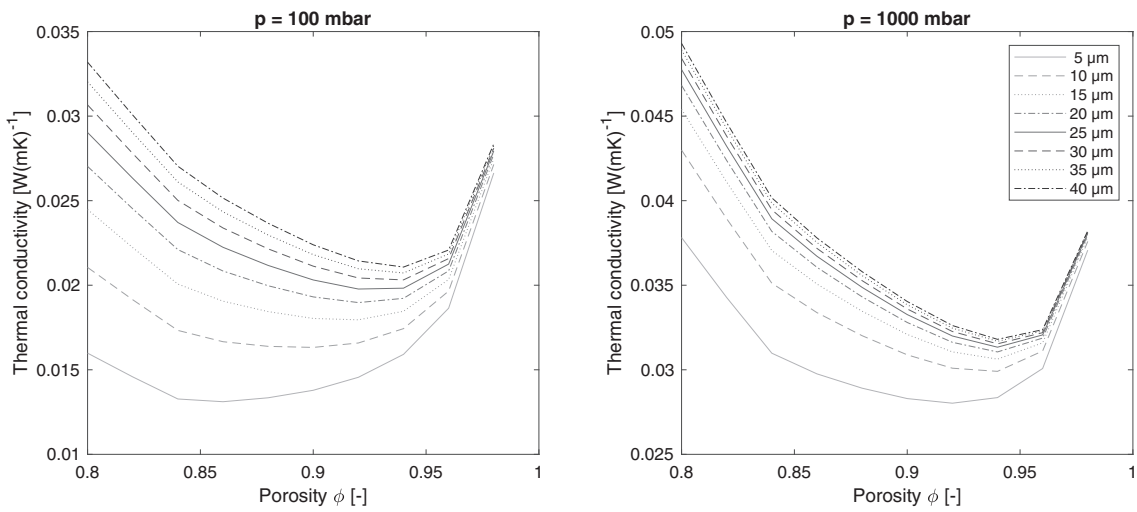
FIGURE 6 Calculated precipitated silica effective thermal conductivity values over porosity for different pressure stages and agglomerate sizes
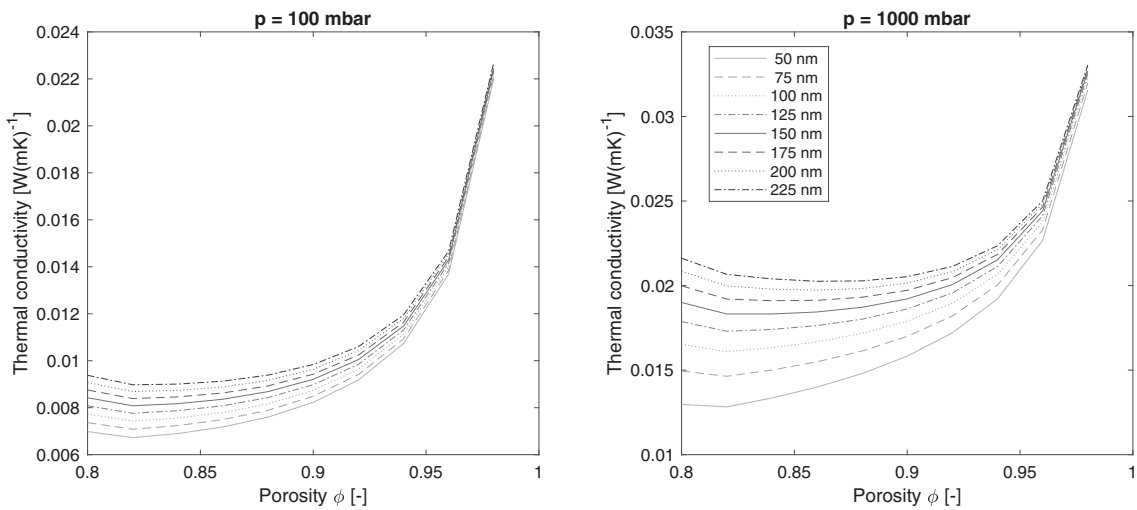

FIGURE 7 Calculated fumed silica effective thermal conductivity values over porosity for different pressure stages and aggregate sizes
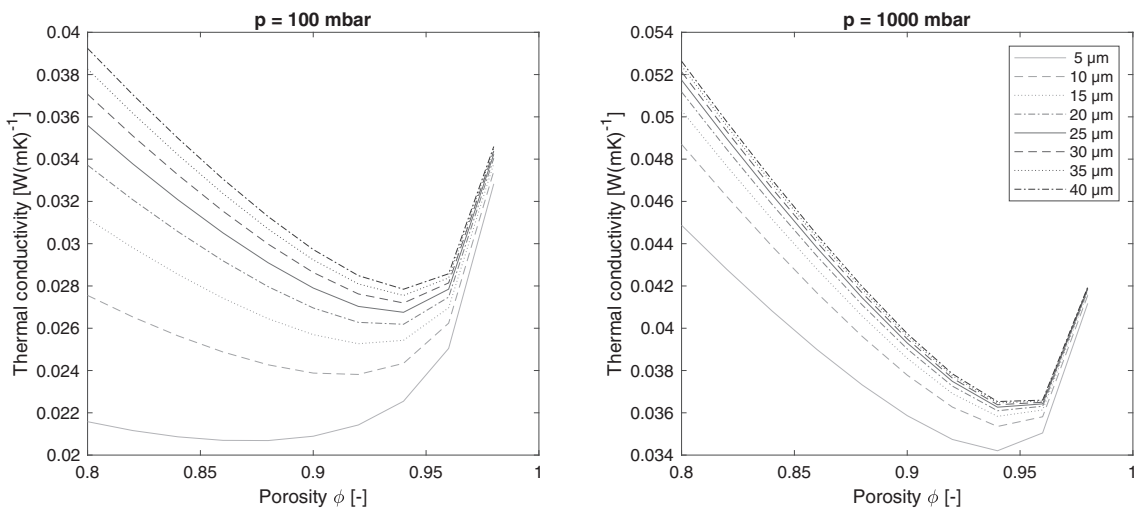

FIGURE 8 Calculated silica gel effective thermal conductivity values over porosity for different pressure stages and aggregate sizes
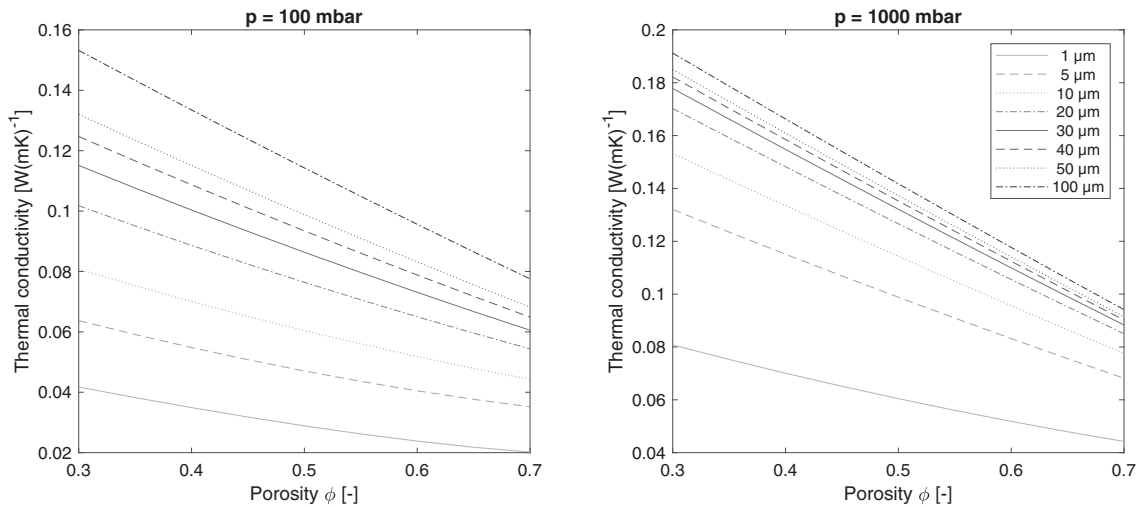
FIGURE 9 Calculated glass spheres' effective thermal conductivity values over porosity for different pressure stages and particle sizes

TABLE 3 Suitability of the different materials for the various applications according to previously defined criteria

Application	Value	PS	FS	SG	GS
Buildings	Particle size	min.	min.	min.	min.
$(\lambda_{100\ \text{mbar}})$	Porosity	0.86	0.82	0.88	max.
	Thermal conductivity $\left[\frac{W}{mK}\right]$	0.0131	0.0067	0.0207	0.0202
Transport boxes	Porosity	0.89	0.89	0.89	0.89
(λ_{base})	Thermal conductivity $\left[\frac{W}{mK}\right]$	0.0049	0.0049	0.0049	0.0049
Atmospheric pressure	Particle size	min.	min.	min.	min.
$(\lambda_{1000\ \text{mbar}})$	Porosity	0.92	0.82	0.94	max.
	Thermal conductivity $\left[\frac{W}{mK}\right]$	0.028	0.0128	0.0342	0.0442
Switchable VIPs	Particle size	max.	max.	max.	max.
$SW = \frac{\lambda(p=1000\ mbar)}{\lambda_{base}}$	Porosity	min.	0.90	0.84	min.
	SW	8.09	4.18	8.82	7.93

related to the denser nature of the SG aggregates, while the PS agglomerates do have a certain intrinsic porosity and small contact points between the aggregates. Due to the fact that the gas thermal conductivity increase strongly with higher porosity, the curves are particularly steep compared to PS for example. This leads to a very small range of optimum porosities. As a consequence, the optimum porosity range would have to be maintained very precisely when using silica gel as the core material.

4.2.4 | Glass spheres

The investigated porosity range is much smaller for glass beads than for the other materials because this material forms a much denser bulk in reality. Therefore, the thermal conductivity at low pressures is primarily characterized by solid thermal conductivity. Here, a reduction in porosity helps to reduce the overall thermal conductivity in a steady manner. In the higher pressure ranges, a very pronounced coupling effect is added which now dominates the total thermal conductivity and thus leads to considerable differences between minimum and maximum pressure.

4.2.5 | Core materials for different applications

To be able to select theoretically optimum core materials for the various applications, the most important properties in each case must be defined. The main criteria for selecting a suitable core material for the various applications were selected as follows:
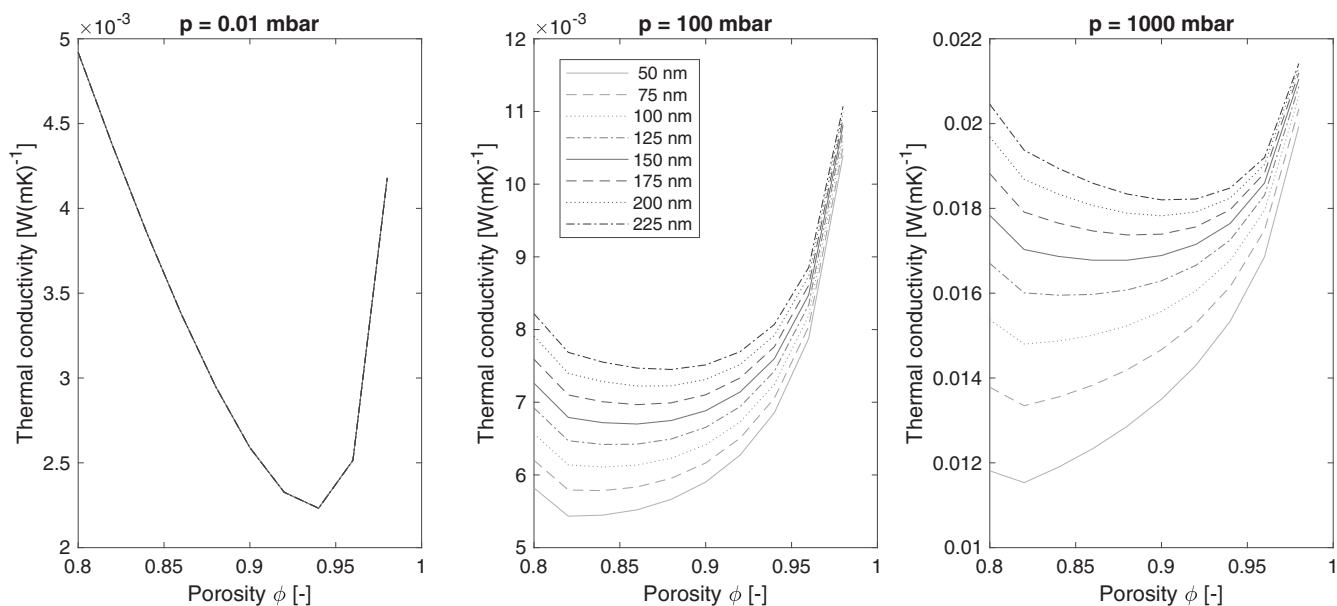
FIGURE 10 Calculated opacified fumed silica effective thermal conductivity values over porosity for different pressure stages and particle sizes

- Building sector:
Even though researchers are working intensively on the development of new and increasingly better high-barrier films for VIPs,[36] a minimum degree of gas diffusion through the envelope can never be avoided. Therefore, in long-term applications, like the building sector, in addition to a low initial thermal conductivity, and the longevity of the VIP is primarily decisive. Since gas diffusion through the barrier film is independent of the VIP-core, the main consideration when selecting the core material is a moderate increase in thermal conductivity with increasing pressure. Therefore, the thermal conductivity at 100 mbar is considered a reference.
- Transport boxes: The packaging industry is the classical example of a VIP with a short life expectancy. Return systems for transport boxes already exist, but despite this, the boards, also due to damage, do not achieve by far the service lives of the VIPs used in the construction sector. Therefore, the decisive parameter here is the initial thermal conductivity, that is, the thermal conductivity at very low pressures λ_{base} immediately after production.
- Atmospheric pressure insulations: Silica-based materials are also suitable for use at atmospheric pressure. They are petroleum-free, non-flammable, pressure-stable, and have low conductivity values. Logically, the thermal conductivity at $P = 1000$ mbar is decisive here.

- Switchable VIPs: In some special applications it can be advantageous to be able to switch the insulation on and off by gas pressure differences. In this case, it is important to find a material with a maximum ratio $\frac{\lambda(p=1000\ mbar)}{\lambda_{base}}$. The desired absolute heat transfer can be adjusted via the material thickness and the pressure.

Of course, in addition to the gas pressure-dependent thermal conductivity, there are other important parameters that can be decisive in the selection of core materials. However, since such influences are difficult to quantify within this framework, they are taken into account only qualitatively when evaluating the results.

Such parameters are, for example, the price per volume or per thermal resistance. In addition, weight is very important in mobile applications like transport boxes. Furthermore, the ability to absorb water molecules and the corresponding effect on the thermal conductivity of the materials must be considered to calculate the service life of the VIP.[37] An equally important criterion for some materials can be processability. For the classic production method, it is necessary to be able to press the core materials into reasonably stable sheets to ensure further processing. This requirement can be even more important for atmospheric pressure applications, where the materials are not placed in a stabilizing vacuum package. Fumed silica is particularly well suited for this purpose, as the particles interlock well due to the hierarchical aggregate structure. This step is usually less successful for

materials with more spherical particles. In this case, alternative production techniques, such as the pouring technique, must be used. However, especially for transport boxes (or also on thermal storage units), this method can be advantageous in combination with free-flowing materials, as it allows the VIPs to remain bendable and thus minimizes edge effects. Moreover, dealing with switchable VIPs it must be possible to aerate and deaerate in as short a time as possible.[38] Furthermore, alternative gases with higher thermal conductivities can be considered for this application to further increase the *SW* factor.[39] However, all these "soft" criteria will be considered only marginally in this work.

The conductivity-related results of the respective categories can be found in Table 3. The first column lists the applications and again the corresponding criteria. The following columns show the relevant material properties and the respective results. The indication of absolute values for the calculated thermal conductivities must be considered with care because the achieved extreme values depend on the freely chosen limits of the parameter studies. Furthermore, the mentioned uncertainty of the calculation models needs to be considered. For example, the minimum thermal conductivity of fumed silica at atmospheric pressure of $0.0128 \frac{W}{mK}$ is, to the authors' current knowledge, a value that has never been met by measurement. It must be taken into account that in reality additional influencing factors not considered here may affect the ETC of the materials. For example, to compress fumed silica to porosity of the calculated 0.84, such high pressures would probably have to be used that the solid heat conduction would increase strongly. It should therefore be mentioned at this point that this is an idealized consideration. Nevertheless, the results give an indication of how the perfect core material would have to be structured for the applications shown.

For the **building sector**, fumed silica is clearly to be favored. The low coupling fraction caused by the small aggregates leads to the smallest increase in thermal conductivity with increasing pressure. The optimum porosity is $\phi = 0.82$, which is comparatively low. This effect can also be explained by the low λ_c. With decreasing porosity, the solid thermal conductivity and the coupling fraction increase, while the radiative conductivity and the gas thermal conductivity decrease. If the coupling conductivity is low due to the small aggregates, the optimum is rather in the direction of smaller porosities. For silica-based insulation materials at **atmospheric pressure**, fumed silica is also the favorite. The reason is the same as for the building sector.

For **transport boxes**, the most important factor is the low initial thermal conductivity of the VIPs. As already mentioned, λ_{base} is the same for all materials under the assumptions made. The most important thing here is to meet the optimum porosity of $\phi = 0.89$ as good as possible. Precipitated silica is therefore proposed as the core material to be favored at this point since it is the comparatively cheapest material. The challenge here, however, is the production of the cores, since the mechanical stability of the compacts during production can only be guaranteed to a limited extent.[40] Possibly contrary to the intuitive assumption, a particularly large spread between minimum and maximum values is not obtained for **switchable VIPs** at high porosities, but rather at low ones. Although the switchable fraction, namely the gas phase, is volumetrically larger at higher porosities, the number of particles and thus the number of contact points is smaller. Especially for materials with spherical microstructures, the most decisive contribution of heat transfer is the coupling between solid and gas phases. This coupling takes place at the contact points. As already discussed in Sonnick et al[34] for precipitated silica, the coupling increases approximately linearly with porosity for constant particle size. This relationship only holds for the technically relevant porosity range shown. The highest ratio between the thermal conductivity at atmospheric pressure and the minimum conductivity is observed for silica gel with a porosity of $\phi = 0.84$, where the difference between PS and SG is not large. Here, therefore, the decision is rather influenced by economic or technical factors again.

4.2.6 | Opacified core materials

In practice, opacifiers are added to the core materials to suppress the heat transfer by radiation in most cases. The reduction of λ_r can possibly lead to a shift of the optimum of the previously investigated parameters. This must be taken into account in the design of core materials. In this study, the emission coefficient of a VIP core material consisting of fumed silica and magnetite as well as silicon carbide was also determined as an example. The mass-specific emission coefficient E_m increases from an average of $12.9 \frac{m^2}{kg}$ to $50.6 \frac{m^2}{kg}$ compared to the pure materials consisting of SiO_2 only. This results in a reduced radiation thermal conductivity and thus a different result of the parameter study which can be seen in Figure 10. The optimum porosity for the building application and the application at atmospheric pressure is still $\phi = 0.82$, while the porosity to be preferred for transport boxes increases significantly, namely to $\phi = 0.94$. However, the optimal porosity range must be observed much more precisely in this case, since λ_{base} increases steeply both just above and just below the optimal porosity. The dependencies on particle size remain unchanged.

5 | CONCLUSION

To calculate the gas pressure-dependent thermal conductivity of porous silica-based materials on the basis of their so-called primary product properties, all heat transfer mechanisms (λ_s, λ_r, λ_g, and λ_c) must be calculated individually and can then be combined with each other. The ideal equations and input parameters vary for different materials. In this paper, parameter studies were performed to determine the influences of porosity and particle size on the gas pressure-dependent thermal conductivity of precipitated silica, fumed silica, silica gel, and glass spheres. The Rosseland approximation was used to calculate the radiative thermal conductivity λ_r. The emission coefficient obtained was measured by infrared spectroscopic methods on the silica-based materials. To calculate the solid thermal conductivity λ_s, a common model based on the Hertz contact theory was used. The sum of the two fractions λ_s and λ_r corresponds to the thermal conductivity at very low gas pressures λ_{base}. It was measured using a vacuum guarded hot plate apparatus and agrees well with the calculated values. The most difficult part to predict is the combination of the thermal conductivity of the gas λ_g and the coupling term λ_c, which is responsible for the increase of the effective thermal conductivity with increasing pressure. It can be calculated from a combination of models for the effective and the gas thermal conductivity which can be taken from.[16] As a result, specific recommendations could be made regarding the type of material and the corresponding material properties in terms of particle size and porosity. Of course, particle size and porosity are inextricably linked in reality. Therefore, it is only possible to a limited extent to vary the two separately in material development. The combinations of material values shown in the parameter studies are therefore initially only fictitious. Crucial findings are shown in Table 3 and are summarized in the following paragraphs (important results are in bold).

5.1 | Building sector and atmospheric pressure application

The parameter studies show a clear advantage of **fumed silica** over the other investigated materials for the construction sector, where a long service life of the VIPs is in focus, as well as for the application at atmospheric pressure. In particular, long durability and low thermal conductivity under atmospheric pressure are achieved when **aggregate size** is chosen **as small as possible** and porosity is set to $\phi = 0.82$. Although the parameter study yields noticeably small absolute values for this

combination, the results for the optimum porosity and particle size are correct and should be considered for future development of appropriate core materials. The small absolute values for fumed silica result from the fact that, in contrast to the other materials, the aggregate size is used instead of the agglomerate size for calculating the effective thermal conductivity. While this approach has significant advantages over using agglomerate size, it generally leads to a slight underestimation of thermal conductivity. The truth probably lies somewhere between the aggregates and the agglomerates, since the coupling effects on both size scales overlap here. However, those on the order of magnitude of the aggregates, that is, roughly in the three-digit nanometer range, clearly predominate for fumed silica. Furthermore, the porosity optimum at 0.82 requires a plausibility check. In future work, it would be helpful to include the effect of the pressure required to achieve a certain porosity and its effect on the solid thermal conductivity to exclude misleading conclusions. Nevertheless, low porosities or high densities can make sense for the building sector. This will slightly increase the initial thermal conductivity, but the increase over time caused by gas thermal conductivity and coupling can be effectively reduced by decreasing the porosity (and thus the average pore size). In addition, the weight is of little importance in the construction sector.

5.2 | Transport boxes

Since λ_{base} in this study depends only on the porosity of the materials, the choice of material for VIPs in the transport sector seems to be irrelevant. Thus, the decision must be made primarily on the basis of economic factors, which is why a clear recommendation is made at this point to use **precipitated silica** for the transport sector. The optimum porosity, in this case, is $\phi = 0.89$. For the same reason, precipitated silica is also the right choice for special applications where the pressure increase due to leakage can be compensated by means of a monitoring system and a built-in vacuum pump.

5.3 | Switchable VIP

For switchable VIPs, the factor between fully vacuumed and fully vented materials is most important. This is about the same for precipitated silica, silica gel, and glass beads, which is why economic factors should also be included in the decision. However, there is a slight tendency for **silica gel** to exhibit the largest switching effect with a factor $SW = 8.82$ at a porosity of $\phi = 0.84$ and **maximum particle size**.

5.4 | Opacified material

Furthermore, it must be taken into account that the optima determined in this work are only valid for the corresponding pure substances. Since additives such as opacifiers are frequently used in practice, the considerations can be adjusted accordingly. The investigation of opacified fumed silica shows that the properties to be preferred may well differ from those of the pure substances. Furthermore, opacifier type and concentration can influence the results significantly. However, the procedure shown can also be applied in unchanged form to materials with modified optical properties. The extension of the parameter study with a focus on opacified materials would therefore be an interesting topic for follow-up research.

DATA AVAILABILITY STATEMENT
The data that support the findings of this study are available from the corresponding author upon reasonable request.

ORCID
Sebastian Sonnick ⓘ https://orcid.org/0000-0003-1625-2782

REFERENCES
1. Wernery J, Mancebo F, Malfait WJ, O'Connor M, Jelle BP. The economics of thermal superinsulation in buildings. *Energy Buildings*. 2021;253:111506. doi:10.1016/j.enbuild.2021.111506
2. Reiss H. K6 superinsulations. *VDI heat atlas*. Berlin, Heidelberg: Springer; 2010:1013-1052.
3. Alotaibi SS, Riffat S. Vacuum insulated panels for sustainable buildings: a review of research and applications. *Int J Energy Res*. 2014;38(1):1-19. doi:10.1002/er.3101
4. Almeida FA, Corker J, Ferreira N, et al. Alternative low cost based core systems for vacuum insulation panels. *Cienc e Tecnol dos Mat*. 2017;29(1):e151-e156. doi:10.1016/j.ctmat.2016.10.002
5. Alam M, Singh H, Brunner S, Naziris C. Experimental characterisation and evaluation of the thermo-physical properties of expanded perlite—fumed silica composite for effective vacuum insulation panel (VIP) core. *Energy Buildings*. 2014;69:442-450. doi:10.1016/j.enbuild.2013.11.027
6. Li CD, Saeed MU, Pan N, Chen ZF, Xu TZ. Fabrication and characterization of low-cost and green vacuum insulation panels with fumed silica/rice husk ash hybrid core material. *Mater Design*. 2016;107:440-449. doi:10.1016/j.matdes.2016.06.071
7. Notario B, Pinto J, Solorzano E, Saja dJA, Dumon M, Rodríguez-Pérez MA. Experimental validation of the Knudsen effect in nanocellular polymeric foams. *Polymer*. 2015;56:57-67. doi:10.1016/j.polymer.2014.10.006
8. Di X, Gao Y, Bao C, Ma S. Thermal insulation property and service life of vacuum insulation panels with glass fiber chopped strand as core materials. *Energy Buildings*. 2014;73:176-183. doi:10.1016/j.enbuild.2014.01.010
9. Li CD, Chen ZF, Wu WP, et al. Core materials of vacuum insulation panels: a review and beyond. *Appl Mech Mater*. Vol 174–177; 2012:1437-1440. Advanced Building Materials and Sustainable Architecture ISBN: 9783037854235, Swizerland: Trans Tech Publications Ltd. doi:10.4028/www.scientific.net/AMM.174-177.1437
10. Zhao S, Siqueira G, Drdova S, et al. Additive manufacturing of silica aerogels. *Nature*. 2020;584(7821):387-392. Number: 7821. Nature Publishing Group. doi:10.1038/s41586-020-2594-0
11. Zach J, Hroudová J, Korjenic A. Environmentally efficient thermal and acoustic insulation based on natural and waste fibers. *J Chem Technol Biotechnol*. 2016;91(8):2156-2161. doi:10.1002/jctb.4940
12. Balo F, Sua LS. Techno-economic optimization model for "sustainable" insulation material developed for energy efficiency. *Int J Appl Ceramic Technol*. 2018;15(3):792-814. doi:10.1111/ijac.12855
13. Resalati S, Okoroafor T, Henshall P, Simões N, Gonçalves M, Alam M. Comparative life cycle assessment of different vacuum insulation panel core materials using a cradle to gate approach. *Build Environ*. 2021;188:107501. doi:10.1016/j.buildenv.2020.107501
14. Knudsen M. Die molekulare Wärmeleitung der Gase und der Akkommodationskoeffizient. *Ann Phys*. 1911;339(4):593-656. doi:10.1002/andp.19113390402
15. Yang M, Sheng Q, Guo L, Zhang H, Tang G. How gas-solid interaction matters in graphene-doped silica aerogels. *Langmuir*. 2022;38(7):2238-2247. American Chemical Society. doi:10.1021/acs.langmuir.1c02777
16. Sonnick S, Erlbeck L, Meier M, Nirschl H, Rädle M. Methodical selection of thermal conductivity models for porous silica-based media with variation of gas type and pressure. *Int J Heat and Mass Transf*. 2022;187:122519. doi:10.1016/j.ijheatmasstransfer.2022.122519
17. Verma S, Singh H. Predicting the conductive heat transfer through evacuated perlite based vacuum insulation panels. *Int J Thermal Sci*. 2022;171:107245. doi:10.1016/j.ijthermalsci.2021.107245
18. Rottmann M, Beikircher T. Pressure dependent effective thermal conductivity of pure and SiC-opacified expanded perlite between 293 K and 1073 K. *Int J Thermal Sci*. 2022;179:107652. doi:10.1016/j.ijthermalsci.2022.107652
19. Bi C, Tang GH, Hu ZJ, Yang HL, Li JN. Coupling model for heat transfer between solid and gas phases in aerogel and experimental investigation. *Int J Heat Mass Transf*. 2014;79:126-136. doi:10.1016/j.ijheatmasstransfer.2014.07.098
20. Singh H, Geisler M, Menzel F. Experimental investigations into thermal transport phenomena in vacuum insulation panels (VIPs) using fumed silica cores. *Energ Buildings*. 2015;107:76-83. doi:10.1016/j.enbuild.2015.08.004

21. Prasolov RS. *Generalization of the equation of the thermal conductivity of gases*. Priborostr: Izv. VUZ'ov; 1961.

22. Kosten CW. The mean free path in room acoustics. *Acta Acustica United with Acustica*. 1960;10(4):245-250.

23. Bauer R. *Effektive radiale Wärmeleitfähigkeit gasdurchströmter Schüttungen mit Partikeln unterschiedlicher Form und Größenverteilung: mit 7 Tafeln*. Düsseldorf: VDI-Verl; 1977.

24. Kaganer MG. Thermal insulation in cryogenic engineering. *Israel Program Sci Transl*. 1969;1:6-21.

25. Fricke J, Lu X, Wang P, Büttner D, Heinemann U. Optimization of monolithic silica aerogel insulants. *Int J Heat Mass Transf*. 1992;35(9):2305-2309. doi:10.1016/0017-9310(92)90073-2

26. Song S, Yovanovich MM. Correlation of thermal accommodation coefficient for 'engineering' surfaces. *ASME HTD*. 1987;69:107-116.

27. Swimm K, Vidi S, Reichenauer G, Ebert HP. Coupling of gaseous and solid thermal conduction in porous solids. *J Non Cryst Solids*. 2017;456:114-124. doi:10.1016/j.jnoncrysol.2016.11.012

28. Reiss H. 3. Approximate solutions of the equation of transer. In: Reiss H, ed. *Radiative Transfer in Nontransparent, Dispersed Media* (Springer Tracts in Modern Physics). Berlin, Heidelberg: Springer; 1988:96-138.

29. Rosseland S. *Astrophysik: Auf Atomtheoretischer Grundlage*. Vol. 11. Berlin Heidelberg: Springer-Verlag; 2013:254.

30. Siegel R, Howell J. *Thermal Radiation Heat Transfer*. New York, NY: Mc GRAW HILL Book Company; 1972.

31. Dietrich B, Fischedick T, Heissler S, Weidler PG, Wöll C, Kind M. Optical parameters for characterization of thermal radiation in ceramic sponges—experimental results and correlation. *Int J Heat Mass Transf*. 2014;79:655-665. doi:10.1016/j.ijheatmasstransfer.2014.08.023

32. Swimm K, Reichenauer G, Vidi S, Ebert HP. Gas pressure dependence of the heat transport in porous solids with pores smaller than 10 microns. *Int J Thermophys*. 2009;30(4):1329-1342. doi:10.1007/s10765-009-0617-z

33. Zehner P, Schlünder EU. Einfluß der Wärmestrahlung und des Druckes auf den Wärmetransport in nicht durchströmten Schüttungen. *Chemie Ingenieur Technik*. 1972;44(23):1303-1308. doi:10.1002/cite.330442305

34. Sonnick S, Meier M, Ross-Jones J, et al. Correlation of pore size distribution with thermal conductivity of precipitated silica and experimental determination of the coupling effect. *Appl Therm Eng*. 2019;150:1037-1045. doi:10.1016/j.applthermaleng.2019.01.074

35. Pramanik S, Manna A, Tripathy A, Kar KK. Current advancements in ceramic matrix composites. In: Kar KK, ed. *Composite Materials*. Berlin, Heidelberg: Springer Berlin Heidelberg; 2017:457-496.

36. Miesbauer O, Kucukpinar E, Kiese S, Carmi Y, Noller K, Langowski HC. Studies on the barrier performance and adhesion strength of novel barrier films for vacuum insulation panels. *Energy Buildings*. 2014;85:597-603. doi:10.1016/j.enbuild.2014.06.054

37. Yrieix B, Morel B, Pons E. VIP service life assessment: interactions between barrier laminates and core material, and significance of silica core ageing. *Energy Buildings*. 2014;85:617-630. doi:10.1016/j.enbuild.2014.07.035

38. Erlbeck L, Sonnick S, Wössner D, Nirschl H, Rädle M. Impact of aeration and deaeration of switchable vacuum insulations on the overall heat conductivity using different core materials and filling gases. *Int J Energy Environ Eng*. 2020;11(4):395-404. doi:10.1007/s40095-020-00356-y

39. Sonnick S, Meier M, Ünsal G, Erlbeck L, Nirschl H, Rädle M. Thermal accommodation in nanoporous silica for vacuum insulation panels. *Int J Thermofluids*. 2020;1-2:100012. doi:10.1016/j.ijft.2019.100012

40. Guesnet E, Bénane B, Jauffrès D, et al. Why fumed and precipitated silica have different mechanical behavior: contribution of discrete element simulations. *J Non Cryst Solids*. 2019;524:119646. doi:10.1016/j.jnoncrysol.2019.119646